PAPER

Check for updates

Polymer-lipid hybrid nanoparticles co-encapsulating fucoxanthin and carbon dots for targeted anti-inflammatory therapy in Alzheimer's disease

J. Horacio Silvestre-Martínez,[a,b] Lorna G. Yañez-Algandar,[a,b] Karina del Carmen Lugo-Ibarra*[c] and Ana B. Castro-Ceseña [ID] *[a,d]

Alzheimer's disease (AD) is a long-term brain disorder characterized by the buildup of proteins like amyloid-beta (Aβ) and Tau. This disease process can start up to 20 years before symptoms such as memory loss, language problems, changes in personality, and eventually dementia appear. Currently, AD has no cure, and available treatments only ease symptoms, making it a major global health concern. Developing new therapies is urgently needed. Nanomedicine presents promising solutions, especially for overcoming challenges like delivering drugs across the blood−brain barrier (BBB). In this study, we explored polymer-lipid hybrid nanoparticles (NPs) decorated with transferrin (Tf) to help them cross the BBB. These NPs were loaded with carbon dots (CDs) and fucoxanthin (Fx), which have antioxidant and anti-inflammatory qualities that may benefit neurodegenerative disease treatment. The resulting nano-particle formulation (NPs-CDFx) had encapsulation efficiencies of 45% for Fx and 10% for CDs, with an average particle size of about 88.74 nm. The safety of these NPs was tested using an *in vitro* model with lipopolysaccharide (LPS) stimulated rat astrocytes, where high cell viability (92.18%) was observed. qPCR analysis showed that NPs-CDFx significantly lowered the expression of genes linked to neuroinflammation and disease progression, such as APP, GFAP, and S100β. To further confirm delivery, the NPs were injected into five-day-old zebrafish larvae, where confocal microscopy detected the CDs' fluorescence in the brain, indicating successful targeted delivery across the BBB. Overall, these findings suggest that the nanoparticles can efficiently deliver therapeutic agents to the brain, reduce neuroinflammatory gene expression, and demonstrate the effectiveness of polymer-lipid hybrid nanoparticles for targeted brain drug delivery.

Introduction

Alzheimer's disease (AD) is a chronic neurodegenerative disorder characterized by progressive memory loss, personality changes, and cognitive decline.[1] It is the most common cause of dementia and primarily affects people over 65 years of age.[2] In 2019, some 55 million people were estimated to have dementia across the world, a figure predicted to increase to 139 million by 2050.[3] One of the most accepted theories of AD is the amyloid cascade, characterized by the abnormal accumulation of beta amyloid (Aβ) and tau protein,[4] which overactivates microglial cells (microglia and astrocytes) producing proinflammatory molecules, such as cytokines, chemokines and reactive oxygen species (ROS), causing neuroinflammation and oxidative stress.[5] These pathological conditions modulate amyloid precursor protein (APP) processing, glial fibrillary acidic protein (GFAP) and S100 calcium-binding protein B (S100β), increasing toxicity.[6,7] These molecular changes in the brain occur gradually and often develop up to 20 years before symptoms appear.[8]

Many aspects of the disease remain incompletely understood. Traditional therapies for AD focus on symptoms and aim to improve behavior and cognitive function, examples include

[a]*Departamento de Innovación Biomédica, Centro de Investigación Científica y de Educación Superior de Ensenada, Baja California (CICESE), Carretera Ensenada-Tijuana No. 3918, Zona Playitas, C.P. 22860, Ensenada, Baja California, Mexico. E-mail: acastro@cicese.mx*
[b]*Centro de Nanociencias y Nanotecnología (CNYN-UNAM), Carretera Tijuana-Ensenada Km 107, C.P. 22860, Ensenada, Baja California, Mexico*
[c]*Universidad Autónoma de Baja California, Facultad de Ciencias Marinas, Carretera transpeninsular Ensenada-Tijuana, S/N Unidad El Sauzal, C.P. 22860, Ensenada, Baja California, Mexico. E-mail: dlugo@uabc.edu.mx*
[d]*SECIHTI-Departamento de Innovación Biomédica, Centro de Investigación Científica y de Educación Superior de Ensenada, Baja California (CICESE), Carretera Ensenada-Tijuana No. 3918, Zona Playitas, C.P. 22860, Ensenada, Baja California, Mexico*

Rivastigmine, Donepezil, Galantamine and Memantine. However, they do not significantly alter disease progression.[9–11] Among recent therapeutic advances, three anti-amyloid monoclonal antibodies have been developed: Donanemab, Aducanumab (discontinued), and Lecanemab. These therapeutic agents have received approval from the U.S. Food and Drug Administration (FDA) and are used to reduce Aβ; however, their clinical benefit remains modest and safety concerns persist.[12–14] In addition to these approaches, other therapeutic and diagnostic strategies have been explored, including stem cell therapy, gene-related interventions, transdermal drug delivery, ultrasound-assisted delivery or imaging methods, blood-derived biomarkers, cerebrospinal fluid analysis and neuroimaging.[11,13,15,16] Despite their potential, these strategies present specific limitations depending on the approach, including safety risk, elevated costs, technical complexity, absence of standardized protocols and a partial understanding of AD, which collectively hinder their widespread clinical implementation.

Most pharmacological agents for AD focus on symptomatic treatment of the disease, making early diagnosis and treatment vital in improving the quality of life of AD patients. Many aspects of the disease remain incompletely understood. Several hypotheses about AD pathogenesis propose that an ideal prevention or treatment strategy should simultaneously target Aβ aggregation, neuroinflammation, and oxidative stress.[17] Crossing the blood–brain barrier (BBB), low drug solubility, and low bioavailability are the main challenges when developing treatments for neurodegenerative diseases.[18]

Numerous strategies have been explored for their potential pharmaceutical applications, with particular interest in compounds derived from the sea. Among these, one major carotenoid present in algae is fucoxanthin (Fx).[19] Fx has shown relevance in immune modulation, exerts anti-inflammatory effects by the activation of NRF2 pathway in macrophages,[20] blocks protein kinase B (Akt)/nuclear factor-kappaB (NF-κB), mitogen-activated protein kinase (MAPKs)/transcription factor (AP)-1 pathways in BV-2 microglial cells[21] and inhibits NLRP3 inflammasome activation and NF-κB in astrocytes,[22] despite these advances, no studies have reported the impact of Fx on reactive astrocyte markers. In this context, the fucoxanthin used in these studies is extracted from algae, rather than commercial sources,[23] although Fx is found in these natural sources, its extraction is a complicated process due to variations in content between batches, limited purity, and the use of environmentally harmful solvents, among other factors.[23–25] Additionally, Fx low water solubility and poor blood brain barrier permeation limit their potential applications when developing a treatment for AD.[26]

One way to avoid these challenges is through the use of nanotechnology and drug delivery systems (DDS), there are different approaches using nanoparticles (NPs) when it comes to treat AD: lipid-based, polymeric, metal-based, carbon-based, mesoporous silica, as well as dendrimers, hydrogels and conjugates, which focuses on enhancing drug efficiency, delivery, improving solubility and reduced toxicity.[27–29] Particularly, polymeric-lipid nanoparticles, which are biocompatible, offer chemical modifications, enhance bioavailability and drug efficacy, while reducing toxicity.[30,31] In this DDS, the drug is encapsulated in the polymeric core and lipids form an outside membrane, stabilizing the NP, preventing fast release of the drug, and increasing circulation half-time *in vivo*.[32,33] To ensure targeted delivery, this DDS can be modified with surface ligands; since the transferrin receptor is highly expressed on brain capillary endothelial cells (BCECs) lining the BBB, using transferrin-conjugated NPs could increase therapeutic efficacy.[34,35] Despite its advantages, this DDS cannot be monitored using conventional imaging techniques during *in vivo* studies. One way to overcome this challenge is to incorporate a fluorescent molecule or nanoparticle. In this regard, CDs are novel materials with unique properties such as fluorescence, very small particle size (<10 nm), low cost, and biocompatibility.[36] Furthermore, CDs alone have shown promising effects in the context of AD, including the inhibition of tau and Aβ protein aggregation downregulation of proinflammatory cytokine levels, and efficacy enhancement when co-administered with other drugs.[37–41] Previously, transferrin conjugation has been employed with carbon dots (CDs), where fluorescence allows for brain visualization and evaluates biodistribution in a zebrafish model.[35,42] Given these specific research needs, the zebrafish serves as a good neurological model due to its genetic similarity to humans, transparent embryology, and capacity for cost-effective, high-throughput screening. Crucially, its blood–brain barrier is structurally and functionally homologous to that of mammals, providing a unique platform for accurately evaluating such neurospecific drug delivery and efficacy.[43–45]

The encapsulation of CDs in NPs represents a promising platform to integrate therapeutic delivery with diagnostic capabilities, so the present study explores for the first time the synergistic effect of Fx encapsulation combined with CDs within a DDS, as a possible theranostic strategy for neuroinflammatory conditions to treat AD. This work explores the anti-inflammatory effects of transferrin (Tf)-functionalized polymer-lipid hybrid nanoparticles loaded with CDs and Fx. This co-encapsulation contributed to improved cytocompatibility, enhanced loading efficiency of the therapeutic compound, and reduced particle size, so to assess the therapeutic potential of this formulation, we determined the encapsulation efficiency, cell viability which increased when both therapeutic agents were co-encapsulated, and also resulted in a reduced particle size, evaluating four key genes involved in neuroinflammation (APP, GFAP, S100β and IL-6) using a lipopolysaccharide (LPS)-stimulated rat astrocyte model. To the best of our knowledge, no previous studies have reported the effect of commercial Fx and CDs on astrocyte inflammatory markers. Additionally, the presence of Tf and CDs allowed us to demonstrate the targeted delivery of the nanoparticles in the brain of a zebrafish, using confocal scanning microscopy.

Materials

The following reagents were used for the transferrin conjugation reaction: CHO-PEG2000-COOH (CLS-PEG) (Nanosoft

Polymers, USA; 3042–2000), 1-ethyl-3-(3-dimethylaminopropyl) carbodiimide (EDC) (Sigma-Aldrich, USA; E7750), N-hydroxysuccinimide (NHS) (Sigma-Aldrich, USA; 130672), holo-transferrin (Sigma-Aldrich, United States of America (USA); T0665), Microsep™ Advance filters (Cytiva/Pall Life Sciences, USA; MCP010C46). For the synthesis of NPs the following reagents were used: citric acid monohydrate (C1909, Sigma Aldrich), fucoxanthin (HY-N2302, MedChemExpress), sodium hydroxide (NaOH, Fermont, 36902), poly(lactic-co-glycolic acid) (PLGA, Nanosoft Polymers, USA; 11088-20-50K), soy lecithin (HSPC) (Nanosoft Polymers, USA; 26372), Phosphate-buffered saline 1X (PBS), TRIzol® (Sigma-Aldrich, USA; 93289) for RNA extraction and tricaine (HY-W011777, MedChemExpress) to anesthetize the fish.

Methods

CLS-PEG-COOH conjugation with holo-transferrin

EDC (100 mM, 100 µL) and NHS (100 mM, 200 µL) solutions were added to the CLS-PEG (1 mM, 600 µL) solution and sonicated for 10 min. Then, transferrin (2 mg mL^{-1}, 600 µL) was added and left under stirring at 200 rpm for 24 h at 22 °C. To concentrate the solution, remove excess water and eliminate free molecules, Microsep™ Advance filters with a molecular weight cut-off (MWCO) of 10 kDa were used to wash the solution by centrifugation at 9000 rpm for 12 min. The resulting solution was resuspended in 1 mL of water and stored for 24 h −80 °C, finally it was lyophilized for another 24 h, at a vacuum pressure of 0.011 mbar and −56 °C, in a FreeZone 1 lyophilizer (Labconco, USA).

Carbon dots synthesis

Carbon dots were synthesized from the thermolysis of 25 g of citric acid monohydrate, in a Lindberg/Blue M oven (Thermo Fisher Scientific) at 180 °C for 40 h.[46] Once cooled and pulverized a brown-orange powder was obtained. A pH 4 solution was obtained by mixing 3 g of CD with 6.6 mL of deionized water, to neutralize the CD solution 5 mL of 5 M NaOH were added. The reaction was carried out at 50 °C in a water bath, with constant stirring at 700 rpm for 40 min. This process modulates the size of the CDs, then the solution was frozen at −80 °C for 24 h and then lyophilized for 31 h.[47]

Hybrid lipid polymeric nanoparticles synthesis

The PLGA-HSPC-CLS-PEG-Tf lipid-polymer hybrid NPs (NPs) were synthesized using a modified nanoprecipitation and self-assembly methodology reported elsewhere.[32,48] Briefly, 20 µL of the CDs 5 mg mL^{-1} and 4 µL of Fx 1000 µM were added to the 400 µL PLGA solution, either alone or combined. The aqueous phase consisted of 12.5 µl of HSPC (1 mg mL^{-1}) and 200 µl of CLS-PEG-Tf (1 mg mL^{-1}) added to 1500 µl of 4% EtOH in a capped amber vial, at 200 rpm and 65 °C to ensure the lipids remained liquid. The organic solution was added to the aqueous lipid solution dropwise (1 mL min^{-1}) at 200 rpm. 2400 µl of MiliQ water was then added, followed by sonication for 5 min in an MH 2800 series ultrasonic bath (Branson

Ultrasonics, USA). Finally, washes were performed to remove free molecules and concentrate the solution using 10 kDa Microsep™ Advance filters and centrifugation at 12 000g for 3, 6, 12, and 18 min. The nanoparticles were physicochemically characterized by the following techniques:

Fourier Transform Infrared Spectroscopy (FTIR) was used to analyze the chemical composition and determine the functional groups of lyophilized NPs, powdered precursors (HSPC, CLS-PEG, Tf, CLS-PEG-Tf, PLGA, and CD), and liquid Fx were analyzed in a Cary 630 spectrophotometer (Agilent Technologies, USA) on ATR mode with a spectral range of 4000 to 500 cm^{-1}, a resolution of 2 cm^{-1}, and 16 scans.

Dynamic light scattering (DLS) was used to determine the hydrodynamic diameter, polydispersity index (PDI), and zeta potential (ζ) of the NPs were studied using a Zetasizer Nano-Zs (Malvern Instruments, UK). NPs were used at a concentration of 100 µg mL^{-1}, with a refractive index of 0.142, PBS as the dispersant, and a temperature of 25 °C in a DT1050 cell. Zeta potential was measured with a DTS1070 cell.

Transmission electron microscopy (TEM) was used to determine the size of the NPs, 10 µL of a solution of the NPs were deposited on a 400-mesh copper grid with a Formvar/carbon membrane for 1 min. Then, the excess was absorbed with filter paper, following a negative staining with 10 µL of a 2% uranyl acetate and incubating for 1 min. After incubation, the excess was removed with filter paper and air-dried at 25 °C for 2 h. The analysis was performed using a Hitachi H-7500 transmission electron microscope (Hitachi, Ltd, Japan) at an accelerating voltage of 80 kV.

Photoluminescence of the CDs and NPs was analyzed in a Hitachi F-7000 model 5J1-0003 fluorescence spectrophotometer, NPs were prepared at a concentration of 1 mg mL^{-1}, while the CDs were prepared in different concentrations in MiliQ water and sonicated for 30 min before measuring. Excitation spectra were obtained in the 280–500 nm range with emission wavelengths of 400, 450, 500, 550, and 600 nm. Emission spectra were measured in the 350–700 nm range with excitation wavelengths of 330, 350, 380, 400, and 450 nm.

Encapsulation of fucoxanthin and CD in hybrid nanoparticles

To break the NPs, 800 µl of 95% methanol was added per gram of lyophilized NPs, the solution was incubated for 1 h in the dark. Finally, the solution was centrifuged at 12 000g for 1 minute before measurement.

The concentration of Fx loaded into the hybrid NPs was determined using a standard calibration curve (1 to 10 µM of free Fx), obtained by reading the optical density (OD) at 450 nm in an Epoch plate reader (BioTek, USA).[49]

The concentration of CDs was determined using a calibration curve (10 to 100 µg mL^{-1}) by measuring the photoluminescence in a fluorescence spectrophotometer at an excitation wavelength of 370 nm.

In both cases, the concentration of the compounds was obtained according to the formula:

$$OD_{encapsulated} = OD_{sample} - OD_{blank} \qquad (1)$$

where $OD_{encapsulated}$ corresponds to the sample (OD_{sample}) minus the reading from methanol used as blank (OD_{blank}).

Cell cultures

Human neonatal foreskin dermal fibroblasts, CCD-1112Sk (American Type Culture Collection, USA; CRL-2429) were grown in Dulbecco's modified Eagle's medium (DMEM) supplemented with 10% fetal bovine serum (FBS) and 1% antibiotic-antimycotic (AA) incubated in a humidified atmosphere with 5% CO2 at 37 °C.

The RA-005 rat astrocyte cell line (IXCells Biotechnologies) was cultured using astrocyte basal medium supplemented with FBS, 1% AA, and astrocyte growth supplement (MD-0039, IXCells Biotechnologies) with the same culture conditions described above.

LPS stimulation

Cells were cultured to 80% confluence before assays. An *in vitro* inflammation model was implemented by adding lipopolysaccharide (LPS) to the cell culture to induce the production of proinflammatory genes. Previous studies by other authors have evaluated different concentrations of LPS,[50,51] we choose 100 ng mL^{-1} of LPS, as it activates inflammatory signaling pathways and maintains cytocompatibility,[52] in order to evaluate the treatments that were applied another 24 h. Cytocompatibility was measured by MTT, 7500 cells were seeded per well in a 96-well plate and incubated for 24 h at 37 °C, 5% CO$_2$, to allow the cells to adhere to the plate. After this time, the medium was removed from each well and replaced with medium prepared with the treatments for another 24 h of incubation.

Citocompatibility was measured by MTT, 7500 cells were seeded per well in a 96-well plate and incubated for 24 h at 37 °C, 5% CO$_2$, to allow the cells to adhere to the plate. After this time, the medium was removed from each well and replaced with medium prepared with the treatments for another 24 h of incubation. A 100 μL of 1× PBS (pH 7.4) were used to wash and avoid the contribution of colour from the treatment, then, 90 μL of medium and 10 μL of MTT (5 mg mL^{-1}) were added to incubate at 37 °C, 5% CO2 for four h. Finally, 100 μL of 0.01 M hydrochloric acid (HCl) with 10% sodium dodecyl sulfate (SDS) was added as a solubilizing solution and incubated for 18 h, after which the plate was read at 570 nm. The percentage of cell viability was calculated using the following eqn (2):

$$Citocompatibility\,(\%) = \frac{OD_{sample} - OD_{blank}}{OD_{control} - OD_{blank}} \times 100 \quad (2)$$

where: OD_{sample} is the value of the treated wells, OD_{blank} is the value of the wells containing the MTT solution without cells, $OD_{control}$ corresponds to the untreated wells.

Gene expression

Extraction of mRNA was performed with TRIzol® following the protocol suggested by supplier. Sample quality and quantity were measured in a Nanodrop 2000 spectrophotometer (Thermo Fisher Scientific Inc., USA). 0.2% agarose gel was used to confirm integrity of the mRNA samples. The qPCR reactions were performed with the Kit GoTaq® 1-Step RT-qPCR System (A6020, PROMEGA), on a MicroAmp™ 96 well optical reaction plate (Thermo Fisher), covered with MicroAmp™ optical adhesive film (Thermo Fisher), the reactions were carried out in a 7500 qPCR system (Applied Biosystems, USA) using a $2^{-\Delta\Delta CT}$ method.[53]

Zebrafish microinjection

All animal experiments were approved by the Bioethics Committee of the Centre for Scientific Research and Higher Education of Ensenada, Baja California. The experiments were conducted according to the approved protocol (ORGA_ACUA_2023_10).

Zebrafish (wild type) were obtained from a local supplier and maintained in a 20 L rectangular fish tank with a recirculating water system, at 27 °C and pH 7.4, NH$_3$/NH$_4^+$ ~0 ppm (mg L^{-1}), NO$_2^-$ ~0 ppm (mg L^{-1}), and NO$_3^-$ 0 ppm (mg L^{-1}). The fish were kept on a 14 h light cycle, followed by 10 h of darkness. Fish health was checked daily, and maintenance was performed every two days by changing 50% of the water and checking parameters weekly. Zebrafish reproduction was done to obtain eggs, which were manually cleaned and incubated at 27 °C until microinjection at 5 days post fertilization (dpf).

To optimise larval handling, a 2% agarose gel was prepared using a groove mold (Z-Molds, World Precision Instruments). Specifically, 25 mL of system water were combined with 0.5 g of agarose and microwaved at 10 second intervals until a clear solution was achieved. The solution was then poured into a 100 mm plate, and the mold was positioned prior to complete solidification.

The Manual Microsyringe Pump (MMP, World Precision Instruments) microinjection equipment was prepared according to the user manual, loading 1 mL of NP solution (Empty, Fx, CD, and CDFx) before anesthetizing the fish with tricaine (0.168 mg mL^{-1}) for 1 minute, and then injecting 16 nL of NPs solution with a pre-pulled glass tip (TIP10FLT), using a non-injected group as control, all the experiments were done in triplicate (3 larvae per sample). After injection, the larvae were transferred to a resting plate and allowed to incubate at 27 °C for 5 h before imaging by confocal microscopy (FV1000 Fluoview, Olympus, filter 430–460 nm).

Results and discussion

CLS-PEG-COOH conjugation with holo-transferrin

In this work, we synthesized polymeric-lipid hybrid nanoparticles conjugated with Tf and loaded with fucoxanthin and CDots, considering that Tf receptor is highly expressed on brain capillary endothelial cells (BCECs) lining the BBB,[54,55] Tf being present on this nanoparticles aims to facilitate drug accumulation on the brain, this strategy could increase drug uptake into the brain as seen in previous reports.[34] To confirm the conjugation, FTIR spectra of free CLSPEG, Tf and CPEGTf were measured. CLSPEG peaks found correspond to the

stretching vibration of the C–H bonds are found at 2880 cm^{-1} and a peak at 1100 cm^{-1} corresponding to the stretching vibration of the –C–O–C– bonds.[56,57] Free Tf bands were attributed to amide II at 1540 cm^{-1}, amide I at 1653 cm^{-1} and amine I bond at 3294 cm^{-1}. The CPEGTf molecule showed the characteristic peaks of Tf, which were found at 1541 cm^{-1}, 1637 cm^{-1} and 3283 cm^{-1} respectively (Fig. 1a). This small shift suggests a chemical conjugation between the carboxylic groups from the CLS-PEG and Tf.[58,59]

NPs physicochemical and morphological characterization

Four different types of nanoparticles were synthesized: empty NPs, NPFx, NPCD, and NPCDFx. The presence of their individual components was confirmed using FTIR spectroscopy. Characteristic absorption peaks included the PLGA carbonyl bonds at 1740 cm^{-1},[60] HSPC fatty acid chains at 2917 and 2850 cm^{-1},[61] and several peaks corresponding to the previously described CPEGTf (Fig. 1b).

The hydrodynamic diameter (D_h) of the nanoparticles varied: empty NPs measured 543.8 ± 45.5 nm, NPFx were 185.6 ± 7.9 nm, NPCD were 123.8 ± 3.73 nm, and NPCDFx were 126.3 ± 7.8 nm. All nanoparticle formulations exhibited a negative ζ-potential ranging from −8.86 to −11.9 mV, indicating no major changes in surface composition, also, this negative value could help avoid unspecific electrostatic interactions with the cell membrane.[62] The polydispersity index (PDI) indicates the size distribution of the NPs, a value >0.7 correspond to a polydisperse sample,[63] in this case, our NPs ranged from 0.166 to 0.679, which is within the expected range for hybrid polymeric lipid nanoparticles[64] (Fig. 2a).

Fluorescence spectroscopy characterization of the CDs revealed a distinct emission peak at 465 nm (blue region) upon excitation at 370 nm. To verify the encapsulation efficiency, the fluorescence intensity of the CDs liberated from the NPs was compared to 10 µg of free CDs (Fig. 2b). Analysis of the supernatant collected confirmed that a significant fraction of CDs was removed (Fig. S1, SI), ensuring that the fluorescence signal detected in the final NPCDFX formulation is attributable to CDs retained within the nanoparticles. Furthermore, control measurements of Fx at the same excitation wavelength (λ_{ex} = 370 nm) showed no spectral interference, confirming that the emission at 465 nm is exclusively attributed to the CDs.

Encapsulation efficiency (EE) of Fx was 27.5% (2.75 µM) when loaded alone. Co-encapsulation with CDs increased the EE of Fx to 45% (4.5 µM). Similar EE of fucoxanthin has been found in PLGA-PEG nanoparticles, this drug delivery system EE is 48.44%,[49] the main difference with our NPs is the lipidic membrane conjugated with transferrin. Similarly, CDs alone showed an EE of 6% (6 µg), which increased to 10% (10 µg) when co-encapsulated with Fx (Fig. 2c).

TEM micrographs revealed spherical nanoparticles surrounded by a lipid layer. The average size observed was 223 nm for Empty NPs (Fig. 2d), 208 nm for NPFx (Fig. 2e), and 88 nm for NPCDFx (Fig. 2f). These results suggest that the co-encapsulation of Fx and CDs produces a synergistic effect and can be explained by the nature of the compounds, Fx is an hydrophobic carotenoid and can be entrapped in the PLGA hydrophobic core, there is a relation between hydrophobic compounds promoting a reduction in NPs size,[65,66] while carboxyl groups from CDs give an hydrophilic property and negative, promoting CDs entrapment between the polymeric core (negative) and the hydrophilic inner lipid membrane.[67] This electrostatic interaction reinforces the stability of the NPs, allowing a higher EE, regulated hydrodynamic diameter, and reduced overall nanoparticle size.[68,69]
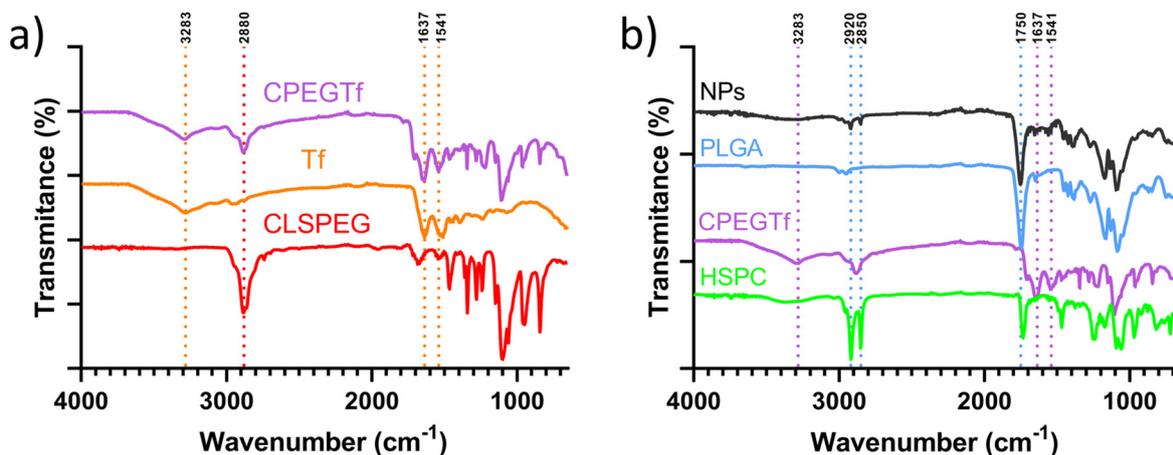

Fig. 1 FTIR spectroscopy characterization of the components and nanoparticle assembly. (a) Spectra of the precursors and the conjugation product: CLSPEG, Tf, and CPEGTf. Successful formation of the CPEGTf conjugate is confirmed by the appearance of the amine stretching band at 3283 cm^{-1}, the amide I band at 1637 cm^{-1}, and the amide II band at 1541 cm^{-1}. (b) Spectra of the nanoparticles (NPs) and their structural components, characteristic functional groups from each precursor are observed: the carbonyl band at 1750 cm^{-1} (PLGA), phospholipid signals at 2920 cm^{-1} and 2850 cm^{-1} (HSPC), and the persistence of the previously described amine and amide bands from the CPEGTf conjugate, confirming its presence within the NPs.
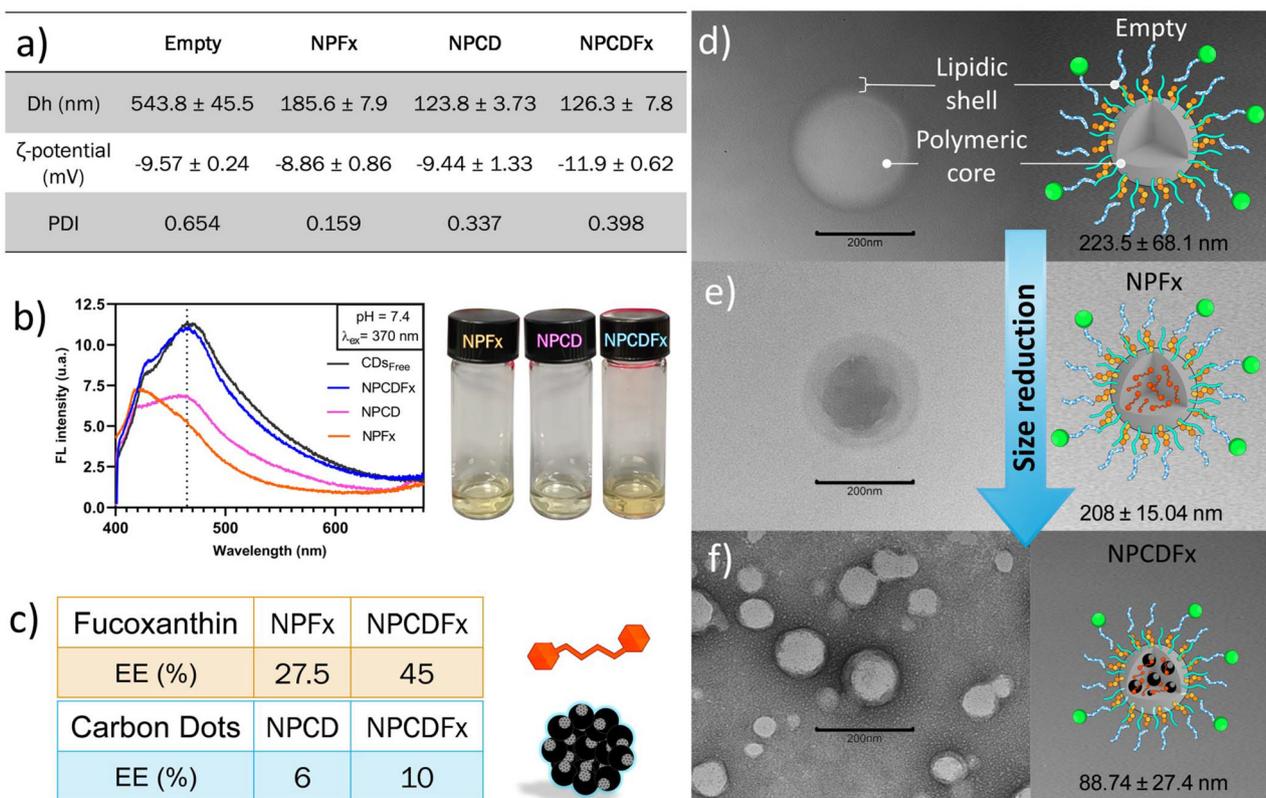
Fig. 2 Physicochemical, optical, and morphological characterization of the nanoparticles. (a) Hydrodynamic diameter (D_h) ζ-potential, and polydispersity index (PDI) of the formulations. Empty NPs exhibit a significantly larger size compared to those encapsulating Fx and CDs. (b) Fluorescence emission spectra (λ_{ex} = 370 nm); the peak at 465 nm confirms the presence of CDs within the NPCDFx system. The intensity of CDs released from the NPs is compared against 10 μg of free CDs to verify encapsulation, while the Fx control shows no spectral interference. (c) Encapsulation efficiency (EE %) of loaded NPs; the co-encapsulation of both therapeutic agents in NPCDFx leads to an increase in EE for both Fx and CDs. (d–f) TEM micrographs of (d) empty NPs, (e) NPFx, and (f) NPCDFx. The images reveal a well-defined spherical morphology with a polymeric core and lipidic shell, highlighting a marked size reduction upon the incorporation of Carbon Dots.

Cell viability of NPs in rat astrocytes

Rat astrocytes (RA-005, iXCells Biotechnologies) were employed to assess the cytocompatibility of both the NPs and the free compounds, using the concentrations previously established in the encapsulation efficiency (EE) experiments. The astrocytes were seeded at a density of 7500 cells mL^{-1} in 96-well plates and pre-treated with 100 ng mL^{-1} of LPS to induce an inflammatory environment.

Upon exposure to the different treatments, only the NPCDFx formulation showed a 92.18% viability, which indicates a protective role under inflammatory stress. In contrast, the other formulations (empty NPs, NPFx, and NPCD) resulted in significantly reduced cell viability, suggesting cytotoxic effects likely due to either the nanoparticle composition, lack of synergistic protection, or concentration-dependent toxicity (Fig. 3a).

These findings suggest that the co-encapsulation of Fx and CDs not only enhances encapsulation efficiency but also contributes to maintaining cell viability under inflammatory conditions, this effect could result from the antioxidant activity of

the CDs and anti-inflammatory properties of the Fx, promoting cell survival by mitigating LPS-induced inflammation.[22,70] Gene expression of four key proinflammatory markers (APP, IL-6, GFAP, and S100β) was evaluated using quantitative PCR (qPCR). These genes were selected based on their well-established association with neuroinflammatory processes, as well as their previous use in related investigations conducted within our research group. In the case of APP mutations in PSEN1 or PSEN2, in astrocytes, alter the proteolytic processing of APP, increasing the ratio and promoting amyloid accumulation in the brain, and also the proinflammation. The GFAP is a biomarker of astrocyte activation that has been proposed as a biomarker of AD and is correlated with the density of Aβ plaques. And for S100β, this protein is abundantly expressed in astrocytes, its levels increase during neuroinflammation and are associated with APP processing.[64]

Rat-specific primers were evaluated to ensure optimal parameters, including melting temperature, amplicon length (bp), GC content (%G/C), and overall specificity (Table S1, SI), as required by the qPCR kit used (GoTaq® 1-Step RT-qPCR System, Promega) (Fig. 3b). Inflammation was confirmed by
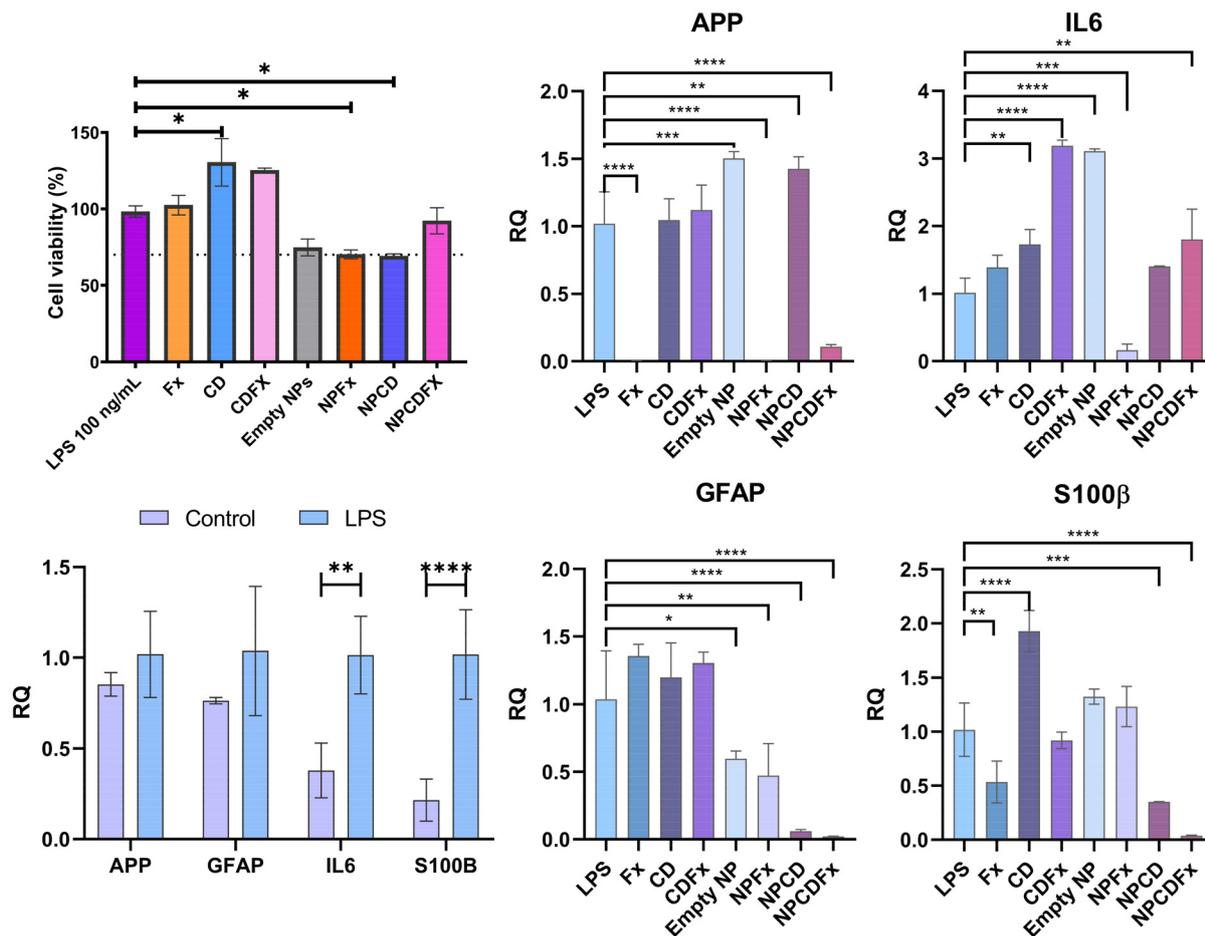
Fig. 3 *In vitro* cytocompatibility and anti-inflammatory efficacy in RA-005 rat astrocytes. (a) Cell viability assessment of free bioactive compounds and NP formulations; among all treatments, only NPCDFx demonstrated high cytocompatibility (92.18% viability), while other formulations fell below the 70% threshold. (b) Validation of the LPS-induced inflammation model, showing a significant upregulation of IL-6 and S100β gene expression. (c) Quantitative PCR (RT-qPCR) analysis of pro-inflammatory and glial markers in LPS-stimulated astrocytes. APP expression was significantly inhibited by Fx, NPFx, and NPCDFx. Pro-inflammatory cytokine IL-6 was downregulated exclusively by NPFx. GFAP expression was modulated by all nanoparticle systems, with NPCDFx exhibiting the highest potency. S100β relative expression was reduced by Fx, NPCD, and NPCDFx. These results suggest that the synergistic effect of the hybrid system enhances the inhibitory mechanism of fucoxanthin on the NF-κB pathway, effectively reducing reactive astrocyte markers. Data is presented as ± SD, $n = 3$ per group, $*p < 0.05$, $**p < 0.01$, $***p < 0.001$, $****p < 0.0001$ (one-way ANOVA followed by Dunnett's *post-hoc* test). Abbreviations: relative quantitation (RQ).

the elevated relative expression (RQ) of IL-6 and S100β genes following stimulation with 100 ng mL^{-1} of LPS (Fig. 3c), this immune response given by microglia and reactive astrocytes is necessary to keep homeostasis in the brain, however, sustained inflammatory conditions helps the development of neurodegenerative diseases.[71] Results on APP relative expression showed a reduction by Fx, NPFx, and NPCDFx treatments. There are some studies highlighting Fx ability to delay oligomer formation of Aβ,[26,72] however there is no background about Fx reducing APP at mRNA level. IL-6 was significantly reduced only by the NPFx treatment, Fx and NPCD showed no difference, any other treatments significantly increased the relative expression. GFAP expression was downregulated by all NP-based treatments, these results could be correlated with the slow release of the compounds from the hybrid NPs,[64,73] studies on post-surgery mice indi-

cates that Fx reduces the number of GFAP positive cells due to the activation of NF-E2-related factor 2 (Nrf2) inducing an antioxidant response,[74] in the case of CDs encapsulated, this study indicates a reduction in expression when administered through a NP formulation. NPCDFx treatment combines the effect of Fx and CDs, further reducing the relative expression of GFAP. S100β expression was increased when CDs alone are evaluated but not when encapsulated in the NPs, expression was also reduced in the Fx and NPCDFx. Among all formulations, NPCDFx significantly downregulated the expression of APP, GFAP, and S100β at the mRNA level, these results suggests that administration through slow release from NPs and the synergistic effect of both compounds, confers a strong anti-inflammatory potential, this effect on the reduction of the APP, GFAP and S100β has not been reported previously (Fig. 3c).

Zebrafish as BBB model microinjection of NPs

Control larvae micrographs did not exhibit fluorescence (Fig. 4a). Similarly, larvae injected with Empty NPs and NPFx showed no detectable fluorescence (Fig. 4b and c, respectively). In contrast, NPCD-injected larvae exhibited fluorescence localized in a structure within the forebrain (Fig. 4d). To enhance visualization of brain distribution, frontal micrographs were taken of larvae injected with NPCDFx. The resulting fluorescence signal confirmed successful delivery and presence of the NPs in the brain region (Fig. 4e).

The emission resulted from the concentration of CDs successfully encapsulated within NPs, which was sufficient to enable tracking of their distribution in the larva zebrafish. Based on our observation and experimentation, the fluorescence intensity associated with the encapsulated CDs was comparable to the obtained 10 μg of free CDs.

Inflammation induced by the addition of lipopolysaccharide (LPS) to primary rat astrocytes, lead to a significant upregulation of proinflammatory markers such as IL-6, APP, S100β, and GFAP, which are indicative of reactive astrocyte states commonly associated with neurodegenerative conditions.[75] Treatment with the hybrid nanoparticles resulted in a marked reduction in the expression of GFAP, APP, and S100β. While previous studies have reported an inhibitory effect of CDs on APP, we did not observe this effect; instead, the contribution of CDs was limited to reducing NP size and allowing higher encapsulation of both therapeutic agents. This, in turn, enhanced the concentration and effect of Fx, our results suggest that Fx an anti-inflammatory effect as reported on other studies,[20] and inhibits IκB phosphorylation, thereby preventing the translocation of the NF-κB transcription factor into the nucleus.[76–78] Although this study focused on IL-6—which did not show a significant reduction—the observed downregulation of APP and glial markers suggests a potent anti-inflammatory effect (Fig. 5). Future research should evaluate TNF-α and IL-1β to further elucidate the scope of this inhibitory mechanism. Importantly, the nanoparticles are conjugated with transferrin, a ligand that facilitates receptor-mediated transcytosis across the blood–brain barrier (BBB).[54] *In vivo* studies in zebrafish suggest that the nanoparticles have the ability to target the BBB, as evidenced by the detectable fluorescence of the CDs within brain tissue, confirming both successful delivery and brain targeting. This multifunctional nanosystem offers a compelling approach for delivering therapeutic agents to the central nervous system and modulating astrocyte-mediated neuroinflammation.
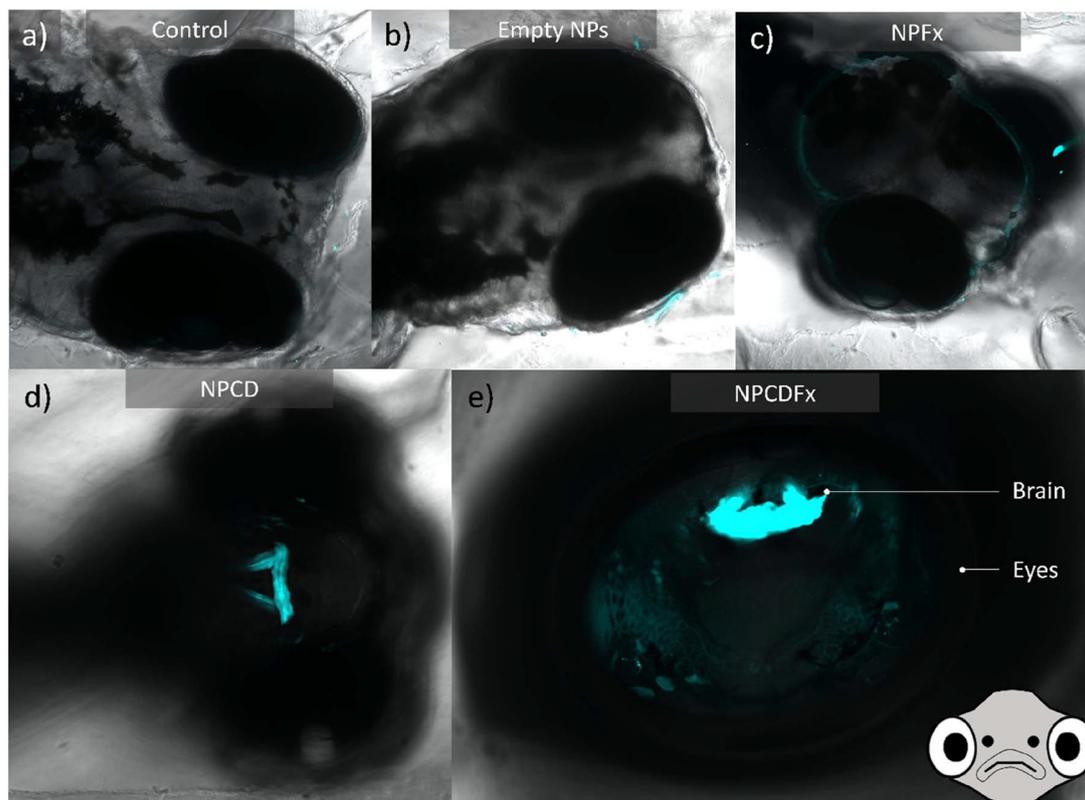

Fig. 4 Confocal fluorescence micrographs of *Danio rerio* 5 hours post-microinjection: (a) control, (b) empty NPs, (c) NPFx, (d) NPCD, and (e) NPCDFx (frontal view). Distinct photoluminescence is exclusively observed in larvae treated with formulations containing CDs (d and e), with a high signal localization in the brain parenchyma. These results suggest that the nanoparticles, functionalized with transferrin, successfully reach the BBB and achieve targeted cerebral accumulation.
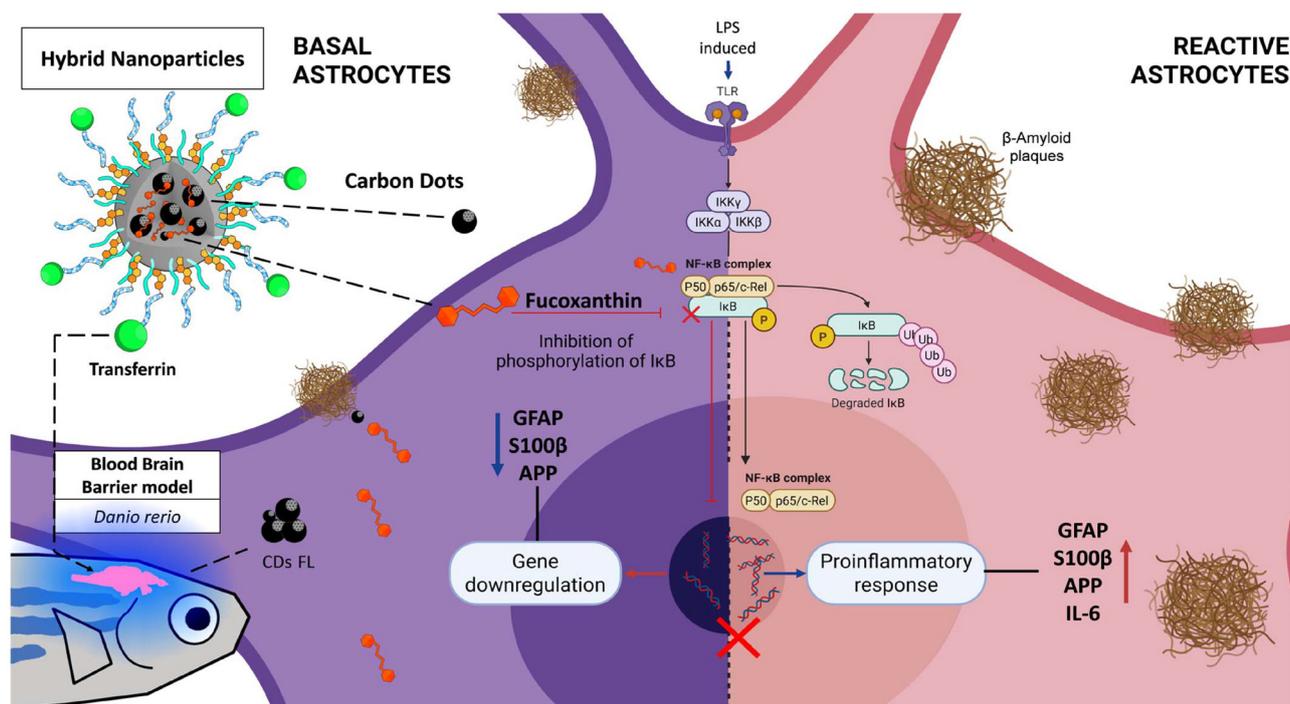
Fig. 5 Graphical representation of the proposed mechanism for the theranostic effect of hybrid nanoparticles in LPS-induced reactive astrocytes. Polymeric hybrid nanoparticles, functionalized with transferrin (Tf) for blood–brain barrier (BBB) targeting, may facilitate the accumulation of the bioactive compounds within the brain: fucoxanthin (Fx) and carbon dots (CDs). In LPS-induced reactive astrocytes, Fx acts by inhibiting the phosphorylation of IκB, thereby preventing the nuclear translocation of the NF-κB transcription factor. This inhibition results in the significant downregulation of pro-inflammatory and glial activation markers, specifically GFAP, S100β, and APP. Simultaneously, the intrinsic fluorescence (FL) of the CDs enables *in vivo* tracking of NPs' distribution within the brain, as demonstrated in the Danio rerio model. Abbreviations: lipopolysaccharide (LPS), toll-like receptor (TLR), inhibitor kappa B kinase (IKK), inhibitor kappa B (IκB), transcription factor p65 (p65), transcription factor (p50), phosphorylation (P), ubiquitination (Ub), glial fibrillary acidic protein (GFAP), S100 calcium-binding protein B (S100β) and amyloid precursor protein (APP). Created in BioRender.

This work contributes to the generation of new knowledge by investigating the synergistic effect of Fx encapsulation and CDs against neuroinflammation. In addition, it addresses one of the major challenges in neurodegenerative diseases and targeted therapy: the BBB. This may facilitate drug delivery, enhance drug bioavailability at the target site, and improve therapeutic efficacy. Furthermore, a potential theranostic nanoparticle could be developed through the encapsulation of CDs, whose fluorescence properties could be exploited for diagnosis and monitoring of therapeutic response. In addition, further studies are required to validate these findings in more complex biological models and *in vivo* systems. Some limitations remain, including the scalability of production processes from laboratory to industrial settings, shelf life studies, and regulatory barriers that may hinder clinical translation.

Conclusions

In this study, polymeric-lipid hybrid nanoparticles functionalised with transferrin (Tf) were developed and thoroughly characterised for the co-encapsulation of carbon dots (CDs) and fucoxanthin (Fx). Physicochemical analysis revealed a stable nanoparticle structure with an optimal hydrodynamic diameter of approximately 88 nm for the NPCDFx formulation, where electrostatic interactions between components supported an encapsulation efficiency of 45% for Fx and 10% for CDs. Biologically, the NPCDFx system displayed excellent cytocompatibility, achieving 92.18% cell viability in rat astrocytes subjected to LPS-induced inflammatory stress, and outperformed both the free molecules and alternative combinations. This notable cytoprotection corresponded to a strong anti-inflammatory response, evidenced by downregulation of key neuroinflammation markers—APP, GFAP, and S100β—a result not previously reported for this synergistic system. While brain accumulation was visualized *via* CDs fluorescence, suggesting Tf-mediated targeting, further studies are required to confirm the integrity of the NPs after crossing the BBB. To advance clinical translation and expand the therapeutic potential of this nanosystem, several research directions are recommended: diversification of animal models to assess pharmacokinetics and biodistribution in rodents (mice or rats), enabling validation of BBB penetration in more complex vascular frameworks and quantification of long-term brain accumulation; optimisation of the formulation by adjusting the polymer-lipid ratio or exploring alternative PEG derivatives to

refine Fx release kinetics and improve colloidal stability for better shelf life; elucidation of underlying molecular mechanisms by investigating signalling pathways such as NF-κB or Nrf2, to uncover further therapeutic targets; and development of advanced imaging protocols to harness CD fluorescence for early diagnosis of neurodegenerative diseases alongside therapeutic delivery. Altogether, these findings establish NPCDFx as a promising multifunctional platform for treating and monitoring neuroinflammatory disorders, thus paving the way for innovative, targeted nanomedicine approaches for central nervous system diseases.

Author contributions

J. Horacio Silvestre-Martínez: conceptualization, methodology, formal analysis, investigation, writing – original draft, and visualization. Lorna G. Yañez-Algandar: methodology and analysis. Karina del Carmen Lugo-Ibarra: conceptualization, methodology, animal protocol and handling, resources, writing – review & editing, supervision and project administration. Ana B. Castro-Ceseña: conceptualization, methodology, resources, writing – review & editing, supervision, project administration, and funding acquisition.

Conflicts of interest

The authors declare that they have no known competing financial interests or personal relationships that could have appeared to influence the work reported in this paper.

Data availability

All data generated during this study supporting its findings are available within the manuscript. All data are available from the corresponding author upon reasonable request.

Supplementary information (SI) is available. See DOI: https://doi.org/10.1039/d6pm00008h.

Acknowledgements

References

1 A. J. Haes, L. Chang, W. L. Klein and R. P. Van Duyne, Detection of a Biomarker for Alzheimer's Disease from Synthetic and Clinical Samples Using a Nanoscale Optical Biosensor, *J. Am. Chem. Soc.*, 2005, **127**, 2264–2271, DOI: 10.1021/ja044087q.

2 F. Leng and P. Edison, Neuroinflammation and microglial activation in Alzheimer disease: where do we go from here?, *Nat. Rev. Neurol.*, 2021, **17**, 157–172, DOI: 10.1038/s41582-020-00435-y.

3 Alzheimer's Disease International, *World Alzheimer Report 2024: Global changes in attitudes to dementia*. London, England: *Alzheimer's Disease International*, 2024; Retrieved from https://www.alzint.org/resource/world-alzheimer-report-2024/.

4 V. Lau, L. Ramer and M.-È. Tremblay, An aging, pathology burden, and glial senescence build-up hypothesis for late onset Alzheimer's disease, *Nat. Commun.*, 2023, **14**, 1670, DOI: 10.1038/s41467-023-37304-3.

5 J. Zhao, W. Bi, S. Xiao, X. Lan, X. Cheng, J. Zhang, D. Lu, W. Wei, Y. Wang, H. Li, Y. Fu and L. Zhu, Neuroinflammation induced by lipopolysaccharide causes cognitive impairment in mice, *Sci. Rep.*, 2019, **9**, 5790, DOI: 10.1038/s41598-019-42286-8.

6 Y. Zhang, H. Chen, R. Li, K. Sterling and W. Song, Amyloid β-based therapy for Alzheimer's disease: challenges, successes and future, *Sig. Transduct. Target. Ther.*, 2023, **8**, 248, DOI: 10.1038/s41392-023-01484-7.

7 T. R. Jay, A. M. Hirsch, M. L. Broihier, C. M. Miller, L. E. Neilson, R. M. Ransohoff, B. T. Lamb and G. E. Landreth, Disease Progression-Dependent Effects of TREM2 Deficiency in a Mouse Model of Alzheimer's Disease, *J. Neurosci.*, 2017, **37**, 637–647, DOI: 10.1523/JNEUROSCI.2110-16.2016.

8 Alzheimer's Association, 2023 Alzheimer's disease facts and figures, *Alzheimers Dement.*, 2023, **19**, 1598–1695, DOI: 10.1002/alz.13016.

9 Alzheimer's Association, *Alzheimers Dement*, Retrieved from https://www.alz.org/alzheimer_s_dementia.

10 S. Mead and N. C. Fox, Lecanemab slows Alzheimer's disease: hope and challenges, *Lancet Neurol.*, 2023, **22**, 106–108, DOI: 10.1016/S1474-4422(22)00529-4.

11 V. V. Sugandhi, D. G. Gadhave, A. R. Ugale, N. Kulkarni, S. N. Nangare, H. P. Patil, S. Rath, R. Saxena, A. Lavate, A. T. Patel, A. Jadhav and K. R. Paudel, Advances in Alzheimer's therapy: Exploring neuropathological mechanisms to revolutionize the future therapeutic landscape, *Ageing Res. Rev.*, 2025, **109**, 102775, DOI: 10.1016/j.arr.2025.102775.

12 J. Wu, C. Geng, L. Liu and Y. Tang, Advancement of disease-modifying therapy of Alzheimer's disease: from the perspective of new revised criteria for diagnosis and staging of Alzheimer's disease, *Med. Plus*, 2025, **2**, 100112, DOI: 10.1016/j.medp.2025.100112.

13 L. M. Chavez-López, J. H. Silvestre-Martínez, K. C. Lugo-Ibarra and A. B. Castro-Ceseña, A comprehensive approach

to Alzheimer's Disease: Exploring Nanotechnology, treatment Innovations, and sex differences, *Brain Res.*, 2025, **1862**, 149718, DOI: 10.1016/j.brainres.2025.149718.

14 J. Zhang, Y. Zhang, J. Wang, Y. Xia, J. Zhang and L. Chen, Recent advances in Alzheimer's disease: mechanisms, clinical trials and new drug development strategies, *Sig. Transduct. Target. Ther.*, 2024, **9**, 211, DOI: 10.1038/s41392-024-01911-3.

15 Y. Pan, L. Li, N. Cao, J. Liao, H. Chen and M. Zhang, Advanced nano delivery system for stem cell therapy for Alzheimer's disease, *Biomaterials*, 2025, **314**, 122852, DOI: 10.1016/j.biomaterials.2024.122852.

16 W. Fu and P. C.-L. Ho, Blood-based biomarkers for Alzheimer's disease: Advances in early detection and monitoring of age-related neurodegeneration, *Ageing Res. Rev.*, 2026, **117**, 103058, DOI: 10.1016/j.arr.2026.103058.

17 F. Mangialasche, A. Solomon, B. Winblad, P. Mecocci and M. Kivipelto, Alzheimer's disease: clinical trials and drug development, *Lancet Neurol.*, 2010, **9**, 702–716, DOI: 10.1016/S1474-4422(10)70119-8.

18 D. Wu, Q. Chen, X. Chen, F. Han, Z. Chen and Y. Wang, The blood–brain barrier: structure, regulation, and drug delivery, *Sig. Transduct.Target. Ther.*, 2023, **8**, 217, DOI: 10.1038/s41392-023-01481-w.

19 Z. Yusof, N. M. H. Khong, W. S. Choo and S. C. Foo, Opportunities for the marine carotenoid value chain from the perspective of fucoxanthin degradation, *Food Chem.*, 2022, **383**, 132394, DOI: 10.1016/j.foodchem.2022.132394.

20 M.-B. Kim, H. Kang, Y. Li, Y.-K. Park and J.-Y. Lee, Fucoxanthin inhibits lipopolysaccharide-induced inflammation and oxidative stress by activating nuclear factor E2-related factor 2 via the phosphatidylinositol 3-kinase/AKT pathway in macrophages, *Eur. J. Nutr.*, 2021, **60**, 3315–3324, DOI: 10.1007/s00394-021-02509-z.

21 D. Zhao, S.-H. Kwon, Y. S. Chun, M.-Y. Gu and H. O. Yang, Anti-Neuroinflammatory Effects of Fucoxanthin via Inhibition of Akt/NF-κB and MAPKs/AP-1 Pathways and Activation of PKA/CREB Pathway in Lipopolysaccharide-Activated BV-2 Microglial Cells, *Neurochem. Res.*, 2017, **42**, 667–677, DOI: 10.1007/s11064-016-2123-6.

22 A.-H. Lee, H.-Y. Shin, J.-H. Park, S. Y. Koo, S. M. Kim and S.-H. Yang, Fucoxanthin from microalgae Phaeodactylum tricornutum inhibits pro-inflammatory cytokines by regulating both NF-κB and NLRP3 inflammasome activation, *Sci. Rep.*, 2021, **11**, 543, DOI: 10.1038/s41598-020-80748-6.

23 S. M. Kim, Y.-J. Jung, O.-N. Kwon, K. H. Cha, B.-H. Um, D. Chung and C.-H. Pan, A Potential Commercial Source of Fucoxanthin Extracted from the Microalga Phaeodactylum tricornutum, *Appl. Biochem. Biotechnol.*, 2012, **166**, 1843–1855, DOI: 10.1007/s12010-012-9602-2.

24 A. Pajot, S. Chollet, E. Nicolau and L. Marchal, Improving the extraction and the purification of fucoxanthin from Tisochrysis lutea using centrifugal partition chromatography, *Algal Res.*, 2023, **74**, 103174, DOI: 10.1016/j.algal.2023.103174.

25 J. Lin, L. Huang, J. Yu, S. Xiang, J. Wang, J. Zhang, X. Yan, W. Cui, S. He and Q. Wang, Fucoxanthin, a Marine Carotenoid, Reverses Scopolamine-Induced Cognitive Impairments in Mice and Inhibits Acetylcholinesterase *in vitro*, *Mar. Drugs*, 2016, **14**, 67, DOI: 10.3390/md14040067.

26 N. Oliyaei, M. Moosavi-Nasab, N. Tanideh and A. Iraji, Multiple roles of fucoxanthin and astaxanthin against Alzheimer's disease: Their pharmacological potential and therapeutic insights, *Brain Res. Bull.*, 2023, **193**, 11–21, DOI: 10.1016/j.brainresbull.2022.11.018.

27 D. Elsori, G. Rashid, N. A. Khan, P. Sachdeva, R. Jindal, F. Kayenat, B. Sachdeva, M. A. Kamal, A. M. Babker and S. A. Fahmy, Nanotube breakthroughs: unveiling the potential of carbon nanotubes as a dual therapeutic arsenal for Alzheimer's disease and brain tumors, *Front. Oncol.*, 2023, **13**, 1265347, DOI: 10.3389/fonc.2023.1265347.

28 N. W. Nabih, H. A. F. M. Hassan, E. Preis, J. Schaefer, A. Babker, A. M. Abbas, M. U. Amin, U. Bakowsky and S. A. Fahmy, Antibody-functionalized lipid nanocarriers for RNA-based cancer gene therapy: advances and challenges in targeted delivery, *Nanoscale Adv.*, 2025, **7**, 5905–5931, DOI: 10.1039/D5NA00323G.

29 N. W. Nabih, M. S. Nafie, A. Babker, H. A. F. M. Hassan and S. A. Fahmy, Recent advances in nano vehicles encapsulating cinnamic acid and its derivatives as promising anti-cancer agents, *RSC Adv.*, 2025, **15**, 20815–20847, DOI: 10.1039/D5RA02640G.

30 S. Koirala and K. Cheng, Lipid and polymeric nanocarriers for siRNA delivery to the brain, *J. Controlled Release*, 2025, **388**, 114286, DOI: 10.1016/j.jconrel.2025.114286.

31 O. A. Alsaidan, M. Elmowafy, K. Shalaby, S. I. Alzarea, D. Massoud, A. M. Kassem and M. F. Ibrahim, Hydrocortisone-Loaded Lipid–Polymer Hybrid Nanoparticles for Controlled Topical Delivery: Formulation Design Optimization and *In vitro* and *In vivo* Appraisal, *ACS Omega*, 2023, **8**, 18714–18725, DOI: 10.1021/acsomega.3c00638.

32 P. Ahmaditabar, A. A. Momtazi-Borojeni, A. H. Rezayan, M. Mahmoodi, A. Sahebkar and M. Mellat, Enhanced Entrapment and Improved *in vitro* Controlled Release of N-Acetyl Cysteine in Hybrid PLGA/Lecithin Nanoparticles Prepared Using a Nanoprecipitation/Self-Assembly Method, *J. Cell. Biochem.*, 2017, **118**, 4203–4209, DOI: 10.1002/jcb.26070.

33 J. M. Chan, L. Zhang, K. P. Yuet, G. Liao, J.-W. Rhee, R. Langer and O. C. Farokhzad, PLGA–lecithin–PEG core–shell nanoparticles for controlled drug delivery, *Biomaterials*, 2009, **30**, 1627–1634, DOI: 10.1016/j.biomaterials.2008.12.013.

34 K. B. Johnsen, A. Burkhart, F. Melander, P. J. Kempen, J. B. Vejlebo, P. Siupka, M. S. Nielsen, T. L. Andresen and T. Moos, Targeting transferrin receptors at the blood-brain barrier improves the uptake of immunoliposomes and subsequent cargo transport into the brain parenchyma, *Sci. Rep.*, 2017, 7, 10396, DOI: 10.1038/s41598-017-11220-1.

35 S. Li, Z. Peng, J. Dallman, J. Baker, A. M. Othman, P. L. Blackwelder and R. M. Leblanc, Crossing the blood–

brain–barrier with transferrin conjugated carbon dots: A zebrafish model study, *Colloids Surf., B*, 2016, **145**, 251–256, DOI: 10.1016/j.colsurfb.2016.05.007.

36 W. Gao, J. He, L. Chen, X. Meng, Y. Ma, L. Cheng, K. Tu, X. Gao, C. Liu, M. Zhang, K. Fan, D.-W. Pang and X. Yan, Deciphering the catalytic mechanism of superoxide dismutase activity of carbon dot nanozyme, *Nat. Commun.*, 2023, **14**, 160, DOI: 10.1038/s41467-023-35828-2.

37 W. Zhang, N. Smith, Y. Zhou, C. M. McGee, M. Bartoli, S. Fu, J. Chen, J. B. Domena, A. Joji, H. Burr, G. Lv, E. K. Cilingir, S. Bedendo, M. L. Claure, A. Tagliaferro, D. Eliezer, E. A. Veliz, F. Zhang, *et al.*, Carbon dots as dual inhibitors of tau and amyloid-beta aggregation for the treatment of Alzheimer's disease, *Acta Biomater.*, 2024, **183**, 341–355, DOI: 10.1016/j.actbio.2024.06.001.

38 Y. Hu, J. Cui, J. Sun, X. Liu, S. Gao, X. Mei, C. Wu and H. Tian, A novel biomimetic nanovesicle containing caffeic acid-coupled carbon quantum dots for the treatment of Alzheimer's disease via nasal administration, *J. Nanobiotechnol.*, 2024, **22**, 642, DOI: 10.1186/s12951-024-02912-8.

39 W. Zhang, N. Kandel, Y. Zhou, N. Smith, B. C. L. B. Ferreira, M. Perez, M. L. Claure, K. J. Mintz, C. Wang and R. M. Leblanc, Drug delivery of memantine with carbon dots for Alzheimer's disease: blood–brain barrier penetration and inhibition of tau aggregation, *J. Colloid Interface Sci.*, 2022, **617**, 20–31, DOI: 10.1016/j.jcis.2022.02.124.

40 N. S. Smith, H. J. Burr, W. Zhang and C. Wang, Development of Diverse Carbon Dots to Inhibit Protein Aggregation in Alzheimer's Disease, *Alzheimers Dement.*, 2024, **20**, e087705, DOI: 10.1002/alz.087705.

41 P. Innocenzi and L. Stagi, Carbon dots as oxidant-antioxidant nanomaterials, understanding the structure-properties relationship. A critical review, *Nano Today*, 2023, **50**, 101837, DOI: 10.1016/j.nantod.2023.101837.

42 X. Han, Z. Jing, W. Wu, B. Zou, Z. Peng, P. Ren, A. Wikramanayake, Z. Lu and R. M. Leblanc, Biocompatible and blood–brain barrier permeable carbon dots for inhibition of Aβ fibrillation and toxicity, and BACE1 activity, *Nanoscale*, 2017, **9**, 12862–12866, DOI: 10.1039/C7NR04352J.

43 S. Saleem and R. R. Kannan, Zebrafish: an emerging real-time model system to study Alzheimer's disease and neuro-specific drug discovery, *Cell Death Discov.*, 2018, **4**, 45, DOI: 10.1038/s41420-018-0109-7.

44 C. Quiñonez-Silvero, K. Hübner and W. Herzog, Development of the brain vasculature and the blood-brain barrier in zebrafish, *Dev. Biol.*, 2020, **457**, 181–190, DOI: 10.1016/j.ydbio.2019.03.005.

45 K. A. Prakash, D. S. Nagmoti, M. S. Borkar, H. K. Pannalal and N. Bandaru, Review on zebra fish as an alternative animal model for neurological studies, *Adv. Adv. Biomark. Sci. Technol.*, 2025, **7**, 320–334, DOI: 10.1016/j.abst.2025.08.005.

46 F. Amato, M. C. P. Soares, T. D. Cabral, E. Fujiwara, C. M. D. B. Cordeiro, A. Criado, M. Prato and J. R. Bartoli, Agarose-Based Fluorescent Waveguide with Embedded Silica Nanoparticle–Carbon Nanodot Hybrids for pH Sensing, *ACS Appl. Nano Mater.*, 2021, **4**, 9738–9751, DOI: 10.1021/acsanm.1c02127.

47 B. C. M. Martindale, G. A. M. Hutton, C. A. Caputo and E. Reisner, Solar Hydrogen Production Using Carbon Quantum Dots and a Molecular Nickel Catalyst, *J. Am. Chem. Soc.*, 2015, **137**, 6018–6025, DOI: 10.1021/jacs.5b01650.

48 R. H. Fang, S. Aryal, C.-M. J. Hu and L. Zhang, Quick Synthesis of Lipid–Polymer Hybrid Nanoparticles with Low Polydispersity Using a Single-Step Sonication Method, *Langmuir*, 2010, **26**, 16958–16962, DOI: 10.1021/la103576a.

49 M. Yang, L. Jin, Z. Wu, Y. Xie, P. Zhang, Q. Wang, S. Yan, B. Chen, H. Liang, C. B. Naman, J. Zhang, S. He, X. Yan, L. Zhao and W. Cui, PLGA-PEG Nanoparticles Facilitate *In vivo* Anti-Alzheimer's Effects of Fucoxanthin, a Marine Carotenoid Derived from Edible Brown Algae, *J. Agric. Food Chem.*, 2021, **69**, 9764–9777, DOI: 10.1021/acs.jafc.1c00569.

50 V. Dozio and J.-C. Sanchez, Profiling the proteomic inflammatory state of human astrocytes using DIA mass spectrometry, *J Neuroinflammation*, 2018, **15**, 331, DOI: 10.1186/s12974-018-1371-6.

51 Y. Chen, Y. Yu, J. Kou, H. Qi, C. Zhang, F. Wang, L. Zhou, X. Liang, K. Xu, C. Zhang, A. Zhang, X. Liu, C. Zhang, G. Gan, J. Sun and X. Zhu, Astrocytic AEG-1 drives neuroinflammation and enhances seizure susceptibility, *Neurobiol. Dis.*, 2025, **212**, 106957, DOI: 10.1016/j.nbd.2025.106957.

52 E. Acaz-Fonseca, A. Ortiz-Rodriguez, I. Azcoitia, L. M. Garcia-Segura and M.-A. Arevalo, Notch signaling in astrocytes mediates their morphological response to an inflammatory challenge, *Cell Death Discov.*, 2019, **5**, 85, DOI: 10.1038/s41420-019-0166-6.

53 T. D. Schmittgen and K. J. Livak, Analyzing real-time PCR data by the comparative CT method, *Nat. Protoc.*, 2008, **3**, 1101–1108, DOI: 10.1038/nprot.2008.73.

54 R. Faresjö, H. Lindberg, S. Ståhl, J. Löfblom, S. Syvänen and D. Sehlin, Transferrin Receptor Binding BBB-Shuttle Facilitates Brain Delivery of Anti-Aβ-Affibodies, *Pharm. Res.*, 2022, **39**, 1509–1521, DOI: 10.1007/s11095-022-03282-2.

55 M. J. Gomes, P. J. Kennedy, S. Martins and B. Sarmento, Delivery of siRNA silencing P-gp in peptide-functionalized nanoparticles causes efflux modulation at the blood-brain barrier, *Nanomedicine*, 2017, **12**, 1385–1399, DOI: 10.2217/nnm-2017-0023.

56 H. Asadi, K. Rostamizadeh, D. Salari and M. Hamidi, Preparation of biodegradable nanoparticles of tri-block PLA–PEG–PLA copolymer and determination of factors controlling the particle size using artificial neural network, *J. Microencapsulation*, 2011, **28**, 406–416, DOI: 10.3109/02652048.2011.576784.

57 D. Yang, J. Zhu, Z. Huang, H. Ren and Z. Zheng, Synthesis and application of poly(ethylene glycol)–cholesterol (Chol–PEGm) conjugates in physicochemical characterization of nonionic surfactant vesicles, *Colloids Surf., B*, 2008, **63**, 192–199, DOI: 10.1016/j.colsurfb.2007.11.019.

58 G. B. Heggannavar, S. Vijeth and M. Y. Kariduraganavar, Preparation of transferrin-conjugated poly-ε-caprolactone nanoparticles and delivery of paclitaxel to treat glioblastoma across blood–brain barrier, *Emergent Mater.*, 2019, **2**, 463–474, DOI: 10.1007/s42247-019-00033-9.

59 M. J. Ramalho, I. D. Torres, J. A. Loureiro, J. Lima and M. C. Pereira, Transferrin-Conjugated PLGA Nanoparticles for Co-Delivery of Temozolomide and Bortezomib to Glioblastoma Cells, ACS Appl, *Nano Mater.*, 2023, **6**, 14191–14203, DOI: 10.1021/acsanm.3c02122.

60 Y. Wang, P. Li and L. Kong, Chitosan-Modified PLGA Nanoparticles with Versatile Surface for Improved Drug Delivery, *AAPS PharmSciTech*, 2013, **14**, 585–592, DOI: 10.1208/s12249-013-9943-3.

61 X. Zhao, C. Shi, X. Zhou, T. Lin, Y. Gong, M. Yin, L. Fan, W. Wang and J. Fang, Preparation of a nanoscale dihydromyricetin-phospholipid complex to improve the bioavailability: in vitro and *in vivo* evaluations, *Eur. J. Pharm. Sci.*, 2019, **138**, 104994, DOI: 10.1016/j.ejps.2019.104994.

62 W. J. Lin and C. W. Liu, Polymeric nanoparticles conjugate a novel heptapeptide as an epidermal growth factor receptor-active targeting ligand for doxorubicin, *Int J Nanomedicine*, 2012, 4749, DOI: 10.2147/IJN.S32830.

63 T. Mudalige, H. Qu, D. Van Haute, S. M. Ansar, A. Paredes and T. Ingle, Characterization of Nanomaterials, *Nanomater. Food Appl.*, 2019, 313–353, DOI: 10.1016/B978-0-12-814130-4.00011-7.

64 A. Vargas-Barona, J. Bernáldez-Sarabia and A. B. Castro-Ceseña, Lipid–polymer hybrid nanoparticles loaded with N-acetylcysteine for the modulation of neuroinflammatory biomarkers in human iPSC-derived PSEN2 (N141I) astrocytes as a model of Alzheimer's disease, *J. Mater. Chem. B*, 2024, 5085–5097, DOI: 10.1039/D4TB00521J.

65 N. Tahir, A. Madni, A. Correia, M. Rehman, V. Balasubramanian, M. M. Khan and H. A. Santos, Lipid-polymer hybrid nanoparticles for controlled delivery of hydrophilic and lipophilic doxorubicin for breast cancer therapy, *Int J Nanomedicine*, 2019, **14**, 4961–4974, DOI: 10.2147/IJN.S209325.

66 J. Jaiswal, A. K. Srivastav, R. Patel and U. Kumar, Synthesis and physicochemical characterization of rhamnolipid fabricated fucoxanthin loaded bovine serum albumin nanoparticles supported by simulation studies, *J. Sci. Food Agric.*, 2022, **102**, 5468–5477, DOI: 10.1002/jsfa.11901.

67 F. Rommasi and N. Esfandiari, Liposomal Nanomedicine: Applications for Drug Delivery in Cancer Therapy, *Nanoscale Res. Lett.*, 2021, **16**, 95, DOI: 10.1186/s11671-021-03553-8.

68 B. Mavroidi, A. Kaminari, E. Sakellis, Z. Sideratou and D. Tsiourvas, Carbon Dots–Biomembrane Interactions and Their Implications for Cellular Drug Delivery, *Pharmaceuticals*, 2023, **16**, 833, DOI: 10.3390/ph16060833.

69 Z. Teng, Y. Luo and Q. Wang, Carboxymethyl chitosan–soy protein complex nanoparticles for the encapsulation and controlled release of vitamin D3, *Food Chem.*, 2013, **141**, 524–532, DOI: 10.1016/j.foodchem.2013.03.043.

70 C. Dong, X. Ma, Y. Huang, Y. Zhang and X. Gao, Carbon dots nanozyme for anti-inflammatory therapy via scavenging intracellular reactive oxygen species, *Front. Bioeng. Biotechnol.*, 2022, **10**, 943399, DOI: 10.3389/fbioe.2022.943399.

71 L.-H. You, C.-Z. Yan, B.-J. Zheng, Y.-Z. Ci, S.-Y. Chang, P. Yu, G.-F. Gao, H.-Y. Li, T.-Y. Dong and Y.-Z. Chang, Astrocyte hepcidin is a key factor in LPS-induced neuronal apoptosis, *Cell Death Dis.*, 2017, **8**, e2676, DOI: 10.1038/cddis.2017.93.

72 S. Xiang, F. Liu, J. Lin, H. Chen, C. Huang, L. Chen, Y. Zhou, L. Ye, K. Zhang, J. Jin, J. Zhen, C. Wang, S. He, Q. Wang, W. Cui and J. Zhang, Fucoxanthin Inhibits β-Amyloid Assembly and Attenuates β-Amyloid Oligomer-Induced Cognitive Impairments, *J. Agric. Food Chem.*, 2017, **65**, 4092–4102, DOI: 10.1021/acs.jafc.7b00805.

73 S. Parveen, P. Gupta, S. Kumar and M. Banerjee, Lipid polymer hybrid nanoparticles as potent vehicles for drug delivery in cancer therapeutics, *Med. Drug Discov.*, 2023, **20**, 100165, DOI: 10.1016/j.medidd.2023.100165.

74 Y. Chen, J. Dong, L. Gong, Y. Hong, C. Hu, Y. Bao, H. Chen, L. Liu, L. Huang, Y. Zhao, J. Zhang, S. He, X. Yan, X. Wu and W. Cui, Fucoxanthin, a marine derived carotenoid, attenuates surgery-induced cognitive impairments via activating Akt and ERK pathways in aged mice, *Phytomedicine*, 2023, **120**, 155043, DOI: 10.1016/j.phymed.2023.155043.

75 J. Kim, I. D. Yoo, J. Lim and J.-S. Moon, Pathological phenotypes of astrocytes in Alzheimer's disease, *Exp. Mol. Med.*, 2024, **56**, 95–99, DOI: 10.1038/s12276-023-01148-0.

76 C. Lee, S. Chen, R. Huang-Liu, S. Gau, Y. Li, C. Chen, W. Chen, C. Wu and Y. Kuan, Fucoxanthin decreases lipopolysaccharide-induced acute lung injury through the inhibition of RHOA activation and the NF-κB pathway, *Environ. Toxicol.*, 2022, **37**, 2214–2222, DOI: 10.1002/tox.23587.

77 Y.-P. Yang, Q.-Y. Tong, S.-H. Zheng, M.-D. Zhou, Y.-M. Zeng and T.-T. Zhou, Anti-inflammatory effect of fucoxanthin on dextran sulfate sodium-induced colitis in mice, *Nat. Prod. Res.*, 2020, **34**, 1791–1795, DOI: 10.1080/14786419.2018.1528593.

78 K.-N. Kim, S.-J. Heo, W.-J. Yoon, S.-M. Kang, G. Ahn, T.-H. Yi and Y.-J. Jeon, Fucoxanthin inhibits the inflammatory response by suppressing the activation of NF-κB and MAPKs in lipopolysaccharide-induced RAW 264.7 macrophages, *Eur. J. Pharmacol.*, 2010, **649**, 369–375, DOI: 10.1016/j.ejphar.2010.09.032.